

# BURIED CHARGE ENGINEERING MODEL: VERIFICATION AND VALIDATION

Len Schwer and Todd Slavik

Schwer Engineering & Consulting Services and Livermore Software Technology Corporation

## 1 Introduction

Livermore Software Technology Corporation (LSTC) recently added an empirically-based model for buried mine blast loading via the keyword \*INITIAL\_IMPULSE\_MINE. This is an engineering model based upon experimental results, much like the air blast engineering model provided by \*LOAD\_BLAST\_ENHANCED. The model is based on the work of Westine, et al. (1985) as presented, and extended, by Tremblay (1998). The implementation is applicable to flat (horizontal) and oblique (angled) target plates consisting of either shell or solid elements.

Westine, et al. (1985) performed a series of buried charge experiments using thick (non-deforming) target plates with a set of impulse plugs inserted into holes drilled in the plate. The impulse plugs were spaced at 10 different ranges from the plate center, and hence angles from the center of the buried charge. Detonation of the buried charge forces the impulse plugs vertically out of the plate and measurement of their speed provides an estimate of the momentum (impulse) provided by the buried charge.

Using groupings of appropriate non-dimensional parameters, Westine, et al. (1985) construct a plot of all their impulse plug data, and some similar data from the literature (Wenzel, 1972), in the form of scaled specific impulse versus scaled distance. This data is then fit to an analytical function. The result is for a given:

- Explosive energy release,  $E$  [J]
- Cross sectional area of the charge,  $A$  [m<sup>2</sup>]
- Soil density,  $\rho$  [kg/m<sup>3</sup>]
- Standoff distance of the target from the center of the charge,  $z$  [m]
- Depth of burial from the soil surface to the center of the charge,  $\delta$  [m]
- Lateral distance to the point of interest,  $d$  [m]

The scaled specific vertical impulse,  $i_v$  is provided at the point of interest,  $P$ . Figure 1 provides a schematic of the buried mine and nomenclature.

## 2 Analytical Extension

Tremblay (1998) provides an analytical extension to oblique plates, the more common configuration for vehicles subjected to mine blast, based on Westine, et al. (1985) horizontal plate results.

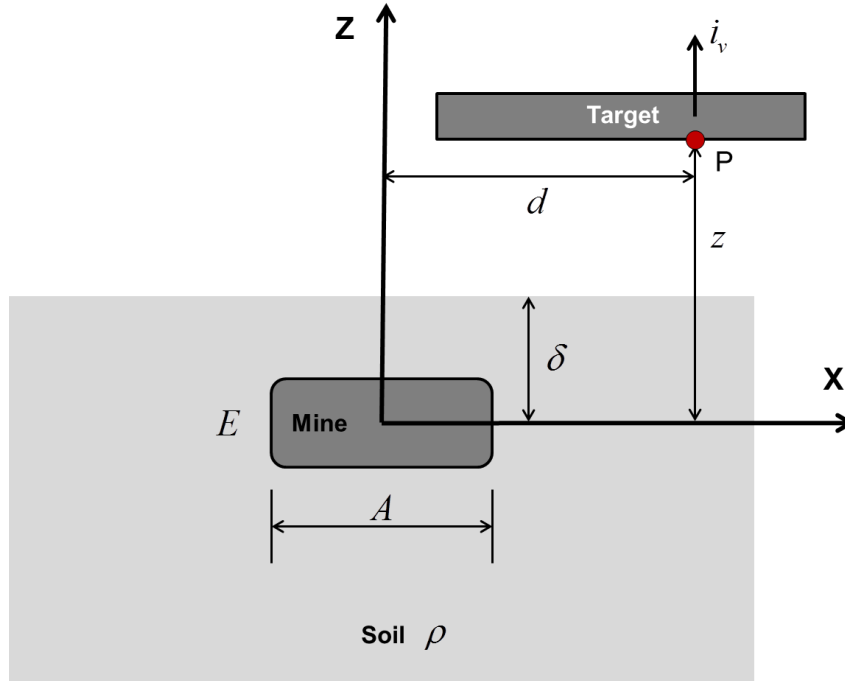


Figure 1 Schematic of the buried mine parameters.

## 2.1 Horizontal Target Plates

Tremblay begins by reintroducing the Westine, et al. impulse data equation with modifications to the nomenclature to suit his subsequent analytical extensions:

$$i_v(x, y) = 0.1352 \left( 1 + \frac{7\delta}{9z} \right) \left( \frac{\tanh(0.9589\zeta d)}{\zeta d} \right)^{3.25} \sqrt{\frac{\rho E}{z}} \quad (1)$$

$$\zeta = \frac{\delta}{z^{5/4} A^{3/8} \tanh \left( \left[ 2.2 \frac{\delta}{z} \right]^{3/2} \right)}$$

Where the specific impulse  $i_v$  has units of stress-time  $\left[ \frac{F}{L^2} T \right]$ , e.g. Pa-s, and  $\zeta$  has units of  $\left[ L^{-1} \right]$ , e.g.  $m^{-1}$  to be consistent with the numerical constants and units prescribed for the quantities identified in Figure 1.

Tremblay also repeats the Westine, et al. limitations on the nondimensional groupings with respect to the range of the applicable data:

$$\begin{aligned}
0.106 &\leq \frac{\delta}{z} \leq 1.0 \\
6.35 &\leq \frac{E/A}{\rho c^2 z} \leq 150 \\
0.154 &\leq \frac{\sqrt{A}}{z} \leq 4.48 \\
0 &\leq \frac{d}{z} \leq 19.3
\end{aligned} \tag{2}$$

The parameter  $c$  in the second inequality is the seismic P-wave speed in the soil expressed in units of  $\left[\frac{L}{T}\right]$  e.g. m/s. Another limitation on Equation (1), omitted by Tremblay, is a factor of 1.8 on the empirical specific impulse that provides users with an assessment of the equation's accuracy, viz.

$$i_v / 1.8 \leq \text{expected impulse} \leq 1.8 i_v \tag{3}$$

i.e. the specific impulse for a given buried charge scenario is bounded below by dividing the predicted specific impulse from Equation (1) by 1.8 and bounded above by the 1.8 times the predicted specific impulse.

Among the items not considered by Westine, et al., and contributing to the above accuracy estimate are the size of the target plate with respect to the points of interest, i.e. *clearing effects* for small targets or the lack of clearing for tracked or wheeled vehicles where the blast is further confined.

Williams and McClennan (2002) determined that a 66% reduction in the Westine et al. impulse produced good correlation with their experimental observations for a 6kg charge of C-4 buried 50mm below the surface with a horizontal target plate at a standoff distance of 406.4mm. They also cite two other examples where the 66% reduction was used to improve the correlation with observations:

“This value of 66% is significant because it is precisely the same value that has been found on two separate occasions with two different target geometries and target materials tested at DRDC Valcartier test range [2,3].”

Williams and McClennan speculate the reason the 66% scaling is needed is because the Westine et al. model does not consider soil type and moisture. However, Westine et al. do consider soil density, which is acknowledged as the primary characteristic for any soil used in buried mine testing or simulations.

Perhaps a more straightforward explanation for the difference between the Williams and McClennan observations, and any particular application of the Westine et al. model, is provided by the accuracy bounds of 1.8 times the model impulse and the model impulse divided by 1.8. Clearly, 0.66 is greater than the lower bound of 0.55(=1/1.8) and thus within the stated model accuracy.

## 2.2 Verification: Horizontal Target - Tremblay's Example 1

To obtain the total impulse on a horizontal target plate requires integrating the specific impulse given by Equation (1) over the area of the plate, i.e.

$$I_v = \iint i_v(x, y) dx dy \tag{4}$$

Tremblay notes there is no analytical solution for the integral of Equation (4) and he proposes an approximate solution. The accuracy of Tremblay's approximate solution is illustrated by an example

where the approximate solution of Equation (4) is compared with the value obtained via Mathematica's function NIntegrate, i.e. a benchmark numerical integration of Equation (4).

The example posed by Tremblay is a one meter square plate subjected to a charge of 6.5kg of TNT covered by 3cm of soil with a density of  $1.6 \text{ kg/m}^3$ . The charge has a diameter of 26.5cm and a height of 8cm. The target plate has a standoff of 40cm from the ground surface. Tremblay reports a total impulse of 17.38 kN-s from his approximate solution and 17.38 kN-s from Mathematica, resulting in a 0.07% difference.

The \*INITIAL\_IMPULSE\_MINE implementation applies Equation (1) to each element segment, multiplies that specific impulse by the known area of the segment, and sums all the element segments specified to determine the total impulse. Both shell and solid (hexahedra) element meshes were constructed taking advantage of the two available symmetry planes, i.e. a quarter model; Note: Tremblay also took advantage of the double symmetry in evaluating his approximate solution. The shell mesh used uniform 20mm elements with a 20mm thickness and the solid element mesh used uniform 10mm elements with two elements through the 20mm thickness; Note: the specific impulses of Westine et al. and Tremblay are independent of the thickness of the target. The LS-DYNA parameters<sup>1</sup> for the \*INITIAL\_IMPULSE\_MINE keyword are:

```
*INITIAL_IMPULSE_MINE
$ SSID      M      RHOS      DEPTH      AREA      SCAL      (not used)  UNIT
   333,    6500.0,  1.60E-3,  70.0,    55.15E3,  0.0,      ,          6
$  X      Y      Z      NIDMC      GVID      TBIRTH      PSID      SEARCH
   0.0,  -70.0,  0.0,    0,        222
```

The shell element model produced an initial vertical speed of 111.7m/s and an initial vertical impulse of 17.53kN-s. The solid element model produced almost identical results for vertical speed of 111.69m/s and a vertical impulse of 17.536kN-s.

Other flat target plate comparisons were made with two of Westine et al. experimental plug results. Good agreement was obtained between the impulse plug measurements and the corresponding \*INITIAL\_IMPULSE\_MINE simulations.

### 2.3 Oblique Target Plates

Figure 2 shows the angles introduced by Tremblay for treating oblique target plates using the known  $i_v$  vertical impulse, i.e. Equation (1), to obtain  $i_n$  the impulse normal to the oblique target plate. As an intermediary, Tremblay introduces  $i_r$  the radial impulse and notes:

$$i_n dA = (i_r \cos \theta)(\cos \theta dA)$$

or  $i_n = i_r \cos^2 \theta$  and similarly  $i_v = i_r \cos^2 \beta$  and combining these two equations provides the desired relation:

$$i_n = i_v \frac{\cos^2 \theta}{\cos^2 \beta} \quad (5)$$

Where  $i_v$  is given as before by Equation (1). Tremblay goes on to compute the total impulse via an approximate solution for the integral of Equation (5) in much the same manner as for the horizontal target plates. Again, the LS-DYNA \*INITIAL\_IMPULSE\_MINE implementation only requires per segment evaluation of Equation (5) as the numerical integration is performed by summing the specific impulses over all the specified element segments.

<sup>1</sup> A description of the keyword parameters is provided in an Appendix.

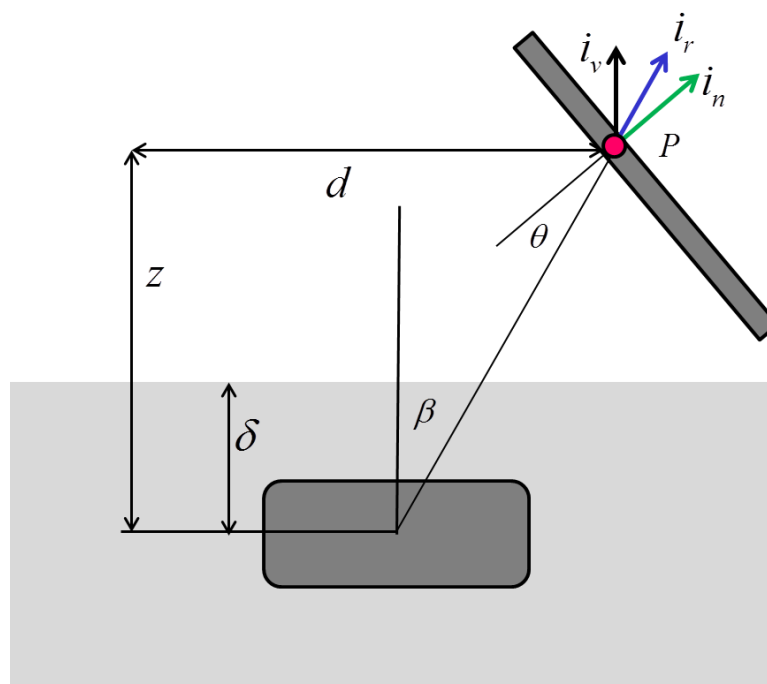


Figure 2 Tremblay's angle nomenclature for oblique targets.

## 2.4 Verification: Oblique Target—Tremblay's Example 7

Consider the V-shaped target plate in Figure 3 where  $\gamma$  varies from 0 (a vertical plate) to 180 degrees (a horizontal plate). The two 1 meter long plates are centered above the mine and the total target has a presented area of  $1\text{m}^2$  on the x-y plane for  $\gamma > 0$ .

Table 1 Comparison of oblique target plate impulses.

$\gamma$ (degree)	Tremblay (kN-s)	*INITIAL_IMPULSE_MINE	
		Shells	Solids
22.5	0.5	0.48	0.42
45	1.7	1.69	1.57
90	5.5	5.54	5.34
135	10.6	10.71	10.40

Table 1 compares Tremblay's analytical impulses for various included angles with the corresponding shell or solid element \*INITIAL\_IMPULSE\_MINE implementation. The largest relative error, -15%, occurs for the  $22.5^\circ$  configuration with solids elements. Some of this relative error may be due to Tremblay only reporting his result to one significant figure, i.e. round off in Tremblay's results.

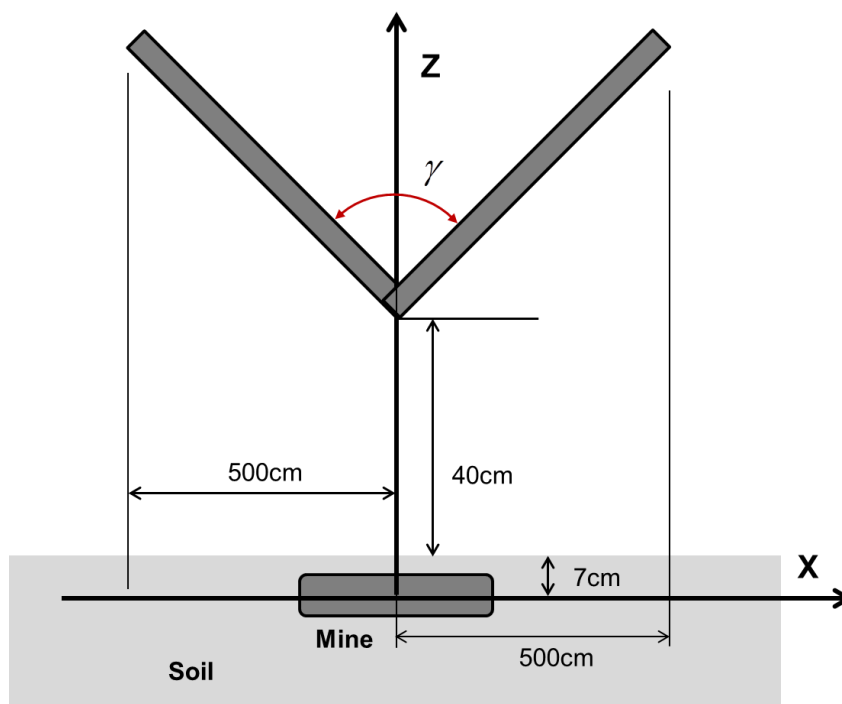


Figure 3 Schematic of oblique target for Tremblay's Example 7.

### 3 Validation – SwRI Buried Charge Experiments

The preceding verification examples provide some confidence that the LS-DYNA impulse algorithm \*INITIAL\_IMPULSE\_MINE was implemented as described by Tremblay. It remains to determine how well the algorithm performs relative to some carefully controlled and documented experiments, i.e. validation experiments.

Anderson et al. (2011) provide a description of replicate testing (3 tests/configuration) of buried charges used to load thick steel plates placed above the soil surface. The three target configurations consist of a horizontal (flat) plate and two “V-shaped” plates with included angles of 120 and 90 degrees. The tests are designed to provide some insight into the underside design of armored personnel vehicles subjected to buried mine blast. The primary experimental diagnostic was the target ‘jump velocity,’ i.e. the initial impulse, derived from the measured maximum vertical displacement of the target plates.

#### 3.1 Brief Description of the SwRI Buried Charge Experiments

A 625g flat cylindrical charge, height 37mm and diameter 113mm, of COMP-B is buried 50mm below the surface of a sand filled cardboard cylindrical tube, i.e. commercially available Sonotube often used as a form for concrete columns. The tubes had a height of 850mm and a diameter of 630mm with a cardboard wall thickness of 3mm and a plywood bottom of unspecified thickness. The cylindrical tubes were apparently placed on top of steel plates covering the ground and reinforced with unspecified steel rings at the top and bottom.

The soil used for the experiments was common silica sand with a grain size of up to 1mm and nominal density of  $1.37 \times 10^{-3} \text{ g/mm}^3$  at a moisture content of 7%. The 7% moisture content was constant for the ‘V-shaped’ plate tests and most of the horizontal plate tests. Measurements were also reported for horizontal plates tested at a 200mm standoff with moisture contents of 14 and 22%.

The horizontal plates were 800x800x60mm with standoff distances of either 200mm or 300mm. For the ‘V-shaped’ plates, constructed from the same size horizontal plates, the standoff was 250mm as

measured from the surface of the sand to the center of gravity of the target plates. Figure 4, from Anderson et al. (2011), shows schematics of the initial configuration for the horizontal and 90 degree target plate experiments.

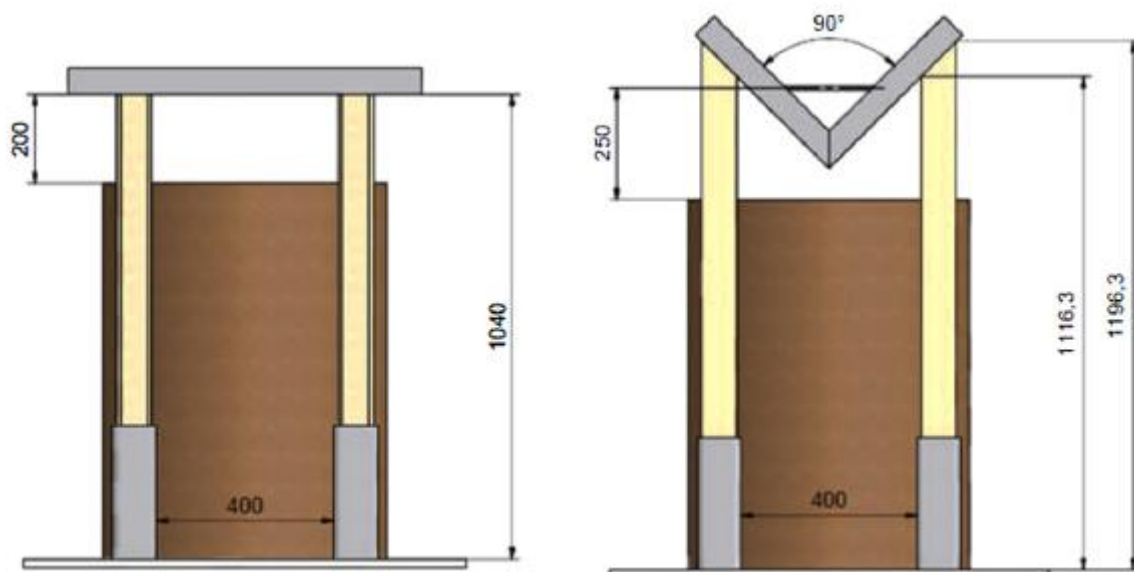


Figure 4 Horizontal (left) and angled 90 degree (right) initial configuration of buried charge experiments; from Anderson et al. (2011).

As an illustration of the quality of the data, Table 2 shows the experimental results for the horizontal plate at 200mm standoff with the 7% moisture sand. The 2% coefficient of variation is quite good, especially considering how variable the sand emplacement and moisture could have been. The experimental measurements for the other target configurations, standoff distances, and sand moisture measurements are similarly quite good.

Table 2 Summary of SwRI momentum measurements for the flat plate configuration.

Shot	Momentum (kg-m/s)
1	1963
2	2025
3	1950
<b>Average</b>	<b>1979</b>
St Dev	40
Coef var	0.02

### 3.2 \*INITIAL\_IMPULSE\_MINE Modeling and Results

As with the Tremblay verification examples, quarter symmetric models consisting of both shells and solid elements were constructed for the three SwRI buried charge configurations. The basic mesh dimension for all three target plates was 8mm. For the quarter symmetric 400x400x60mm plates this means 50x50 shell elements and 50x50x7 solid elements.

The solid element angled plates were constructed based on the 180 degree (horizontal) plates with a modification of the centerline edge to conform to the appropriate included angle, i.e. 45-degrees for the 90-degree included angle<sup>2</sup>. Figure 5 shows an edge and isometric view of the 90-degree solid element target plate. Note: the element segments along the top surface were not square but rather 8x6.8mm rectangles due to include the 45-degree bevel in the target.

<sup>2</sup> When shell elements are joined at an apex, some adjustment of the shell thickness at the apex may be necessary.

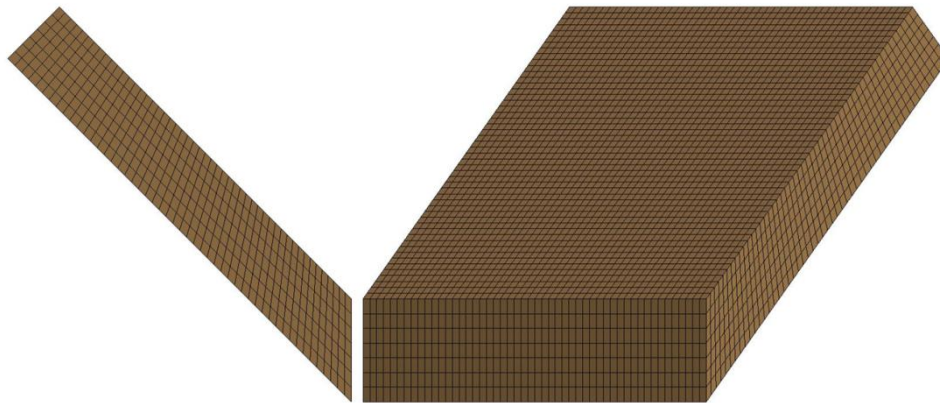


Figure 5 Solid element model for 90-degree SwRI plate.

Omitted from the angled plate models were the three small bracing plates SwRI included in the experiments. While these plates could have been added to the model, no information on their dimensions was provided by SwRI. The nominal steel density of  $7.85 \times 10^{-3} \text{ g/mm}^3$  was used for the 180-degree (horizontal) target plate's mass of 300kg. However, the density was modified for the two angled plates, see Table 3, to obtain the reported masses of 309.4 and 308.4kg for the 120 and 90-degree target plates, respectively.

Table 3 Adjusted densities for SwRI angled plates (mass in kg and density in  $\text{g/mm}^3$ ).

Target Plate	120	90
Mass	309.4	308.4
Shells	$8.0572 \times 10^{-3}$	$8.0313 \times 10^{-3}$
Solids	$8.4220 \times 10^{-3}$	$8.6820 \times 10^{-3}$

The solid element angled plates were positioned with the help of the LS-DYNA pre and post processor, LS-PrePost, which reports the coordinates of the center of gravity for a selected part. After positioning the solid element angled targets, the shell element targets were positioned so the apex of the shell model was aligned with the bottom apex of the solid element model.

Consider for example the 180-degree horizontal target plate. The bottom surface of the 60mm thick target is prescribed to be 200mm above the soil surface. The corresponding shell element model also needs to be placed at 200mm above the surface of the soil, regardless of the associated shell element thickness representing the target plate thickness. If the shell model was located at the mid-plane of the solid model, it would be an additional 30mm away from the soil surface, and the explosive charge. This change in range will change the applied impulse.

The applicability of \*INITIAL\_IMPULSE\_MINE, as per Westine et al. Equations (2), to the SwRI flat plate experiment was confirmed using the following parameters

COMP-B

Mass — 0.625 Kg

Heat of Detonation — 5.02 MJ/Kg

Energy Release —  $3.135 \times 10^6 \text{ J}$

TNT Equivalence (Westine et al.) 1.14

Equivalent Energy Release —  $E = 3.577 \times 10^6 \text{ J}$

Charge Area —  $A = 0.1 \text{ m}^2$

Soil Density —  $\rho = 1370 \text{ Kg/m}^3$

Wave Speed —  $c = 330 \text{ m/s}$

Depth of Burial —  $\delta = 0.05 \text{ m}$

Standoff to Charge Center —  $z = 0.25 \text{ m}$

Lateral Distance (maximum) —  $d = 0.40\sqrt{2} = 0.566 \text{ m}$

The resulting non-dimensional parameter bounds are provided in Table 4.

Table 4 Westine et al. data applicability bounds from Equation (2).

Minimum	Parameter Group	Maximum
	$\delta / z$	
0.106	0.20	1.0
	$(E / A) / (\rho c^2 z)$	
6.35	9.562	150.0
	$\sqrt{A} / z$	
0.15	0.401	4.48
	$d / z$	
0.0	2.263	19.3

The \*INITIAL\_IMPULSE\_MINE keyword parameters for the 180-degree horizontal target plate are:

```
*INITIAL_IMPULSE_MINE
$ SSID      M      RHOS      DEPTH      AREA      SCAL  (not used)  UNIT
  100,    653.13,  1.37E-3,  68.5,    10028.75,  0.0,      ,      6
$  X      Y      Z      NIDMC      GVID      TBIRTH      PSID      SEARCH
   0.0,  -68.5,  0.0,    0,      222,      ,      ,      0.0
```

Note: the equivalent mass of TNT is 653.13g which is 1.045 times the SwRI COMP-B mass of 625g, this is the ConWep equivalence between COMP-B and TNT. There are many equivalencies for TNT and COMP-B as indicated in Table 5.

Table 5 Illustration of TNT equivalencies for COMP-B.

Method	Equivalency
Specific Energy (same as Westine, et al. or Smith & Hetherington, 1994)	1.148
Equivalent Pressure	1.11
Equivalent Impulse	0.98
Chapman-Jouguet Detonation Speed	1.31
Heat of Detonation (Dobartz, LLNL)	1.09
ConWep	1.045

Any of these equivalencies can be used, but none are correct because they all depend on the range at which the pressure/impulse comparison is made, and the total amount of explosive, i.e. small and large charges will have different equivalencies. The reader needs to keep in mind this is an *engineering model*, and the TNT equivalence should be treated as a numerical parameter to be varied in making any important predictions using the model.

Table 6 presents comparisons of the vertical velocity and impulse for the three SwRI plate configurations with the corresponding \*INITIAL\_IMPULSE\_MINE (IIM) shell and solid element models. The results indicate that shell and solid element models provide nearly identical velocity and impulse results.

The largest relative error (RE) is for the 180-degree (horizontal) target plate where the \*INITIAL\_IMPULSE\_MINE result over predicts the SwRI experimental result by 53%. Although this is a large relative error it is within the accuracy bounds suggested by Westine et al., recall Equation (3) and note the upper bound relative error is 180%.

Table 6 Comparisons of SwRI and IIM vertical velocity and impulses.

180	Velocity (m/s)	RE	Impulse (kg-m/s)
SwRI	6.60		1979.33
IIM			
Shells	10.09	0.53	3027.48
Solids	10.09	0.53	3027.50
120	Velocity (m/s)	RE	Impulse (kg-m/s)
SwRI	3.81		1181.67
IIM			
Shells	4.34	0.14	1342.76
Solids	4.34	0.14	1342.76
90	Velocity (m/s)	RE	Impulse (kg-m/s)
SwRI	2.63		812.33
IIM			
Shells	2.07	-0.21	639.32
Solids	2.07	-0.21	639.12

Interestingly, the \*INITIAL\_IMPULSE\_MINE algorithm also over predicts the 120-degree target plate impulse but only by 14%, while the 90-degree target plate impulse is under predicted by 21%. One possible explanation for the over predictions at 180 and 120-degrees, versus an under prediction at 90-degrees, is the effect of clearing on the total impulse. The more horizontal plates, i.e. 180 and 120-degree, provide more vertical confinement for the soil ejecta and detonation products, while the 90-degree plate allows for significant lateral deflection of this material. Note also, these target plates are symmetric about the vertical axis, any energy directed toward the centerline is balance by the symmetry of the targets. Thus only energy directed vertically contributes to the motion of the target plates. This point is also demonstrated by the magnitude of the impulse measured by SwRI for the three target plate configurations, with the largest impulse for the 180-degree plate and the smallest for the 90-degree plate.

#### 4 Comparisons with Multi-Material Arbitrary Lagrange Eulerian (MM-ALE) Models

In a companion document, Anderson et al. (2010) provide numerical simulations, using the Eulerian code CTH (1990), applied to the above described buried charge experiments. In addition to their three dimensional simulations, Anderson et al. note the advantages of approximating the experimental geometry as axisymmetric in an effort to more efficiently quantify numerical grid convergence, i.e. numerical error due to spatial discretization. The use of axisymmetric models whenever possible is clearly good advice. Obviously for the 120 and 90-degree target plates, axisymmetric models do not represent the experimental configuration. However, for the 180-degree plate an equivalent area circular plate is a reasonable replacement for the square plate used in the SwRI tests. The LS-DYNA axisymmetric MM-ALE simulations and parameter studies are described in an appendix.

In this section, 3D MM-ALE models of the SwRI experiments are constructed and the results compared with both the SwRI 3D simulations results and the previously described \*INITIAL\_IMPULSE\_MINE results.

#### 4.1 3D MM-ALE Models

When constructing 3D Eulerian models, there needs to be a balance between mesh refinement (numerical accuracy) and computational cost, i.e. CPU time. All planes of symmetry need to be used and a judicious selection of the overall domain size is critical. For example, the domain used in the present 3D simulations is 900x900x1450mm, for a quarter symmetric model, and a *uniform* 10mm/side mesh would contain  $90 \times 90 \times 145 = 1,174,500$ . A reduction in this number of elements, by a factor of almost 9, can be obtained using a so called 'butterfly' mesh, i.e. a radial mesh with a square at the center.

Figure 6 shows the computational domain used in the 3D MM-ALE models of the SwRI experiments. The right side of this figure shows the overall computation domain which is 900mm wide, and the same dimension into the plane of the paper, and 1450mm tall. The small red region is the COMP-B explosive charge which is surrounded by the sand (green). The sand is surrounded (blue) by what is termed the lower air, and above this area the yellow upper air and the 180-degree target plate in outline. The air domain is divided into two parts to allow for easy visualization of any 'leakage' of the (lower) air into the Lagrange target domain. Note: the Sonotube, and its upper and lower supporting rings, are ignored in this model.

The left portion of Figure 6 shows a horizontal slice through the model. The 'butterfly' mesh consists of a central square region from which the radial mesh lines radiate. The orthogonal mesh is completed by numerous concentric rings whose intersection with the radial lines forms the nodes of the mesh. In the vertical direction, a uniform mesh size of 10mm was selected. The total number of Eulerian elements for this model is 132,675. Note: a further reduction in the number of elements could have been obtained by using a geometric ratio of element sizes in the radial direction in the air domain.

The boundary conditions for this model are no motion normal to the two symmetry planes and no vertical motion at the bottom of the model. The outer circular boundary has a prescribed pressure of one atmosphere to equilibrate the initial pressure in the air domain.

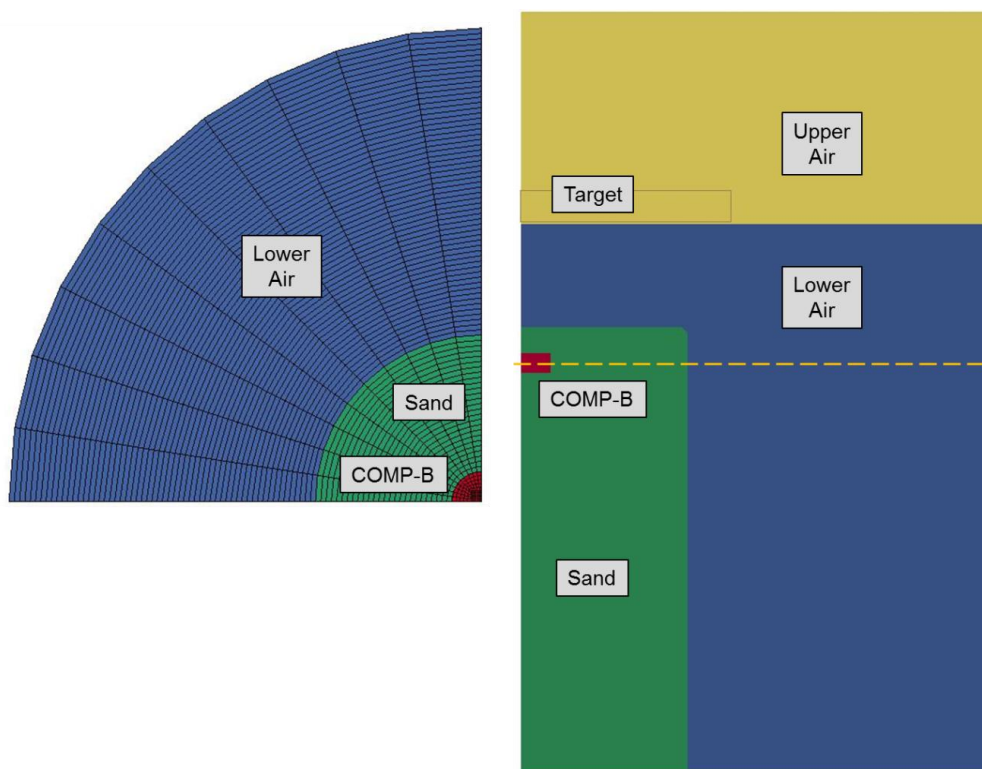


Figure 6 Illustration of butterfly (left) mesh used to construct the quarter symmetric 3D MM-ALE SwRI experiment models.

The target plates are the same Lagrangian solid models used in the \*INITIAL\_IMPULSE\_MINE simulations, i.e. 400x400x60mm with nearly uniform 8mm mesh spacing. The Lagrangian target plates are coupled to the Eulerian domain using the LS-DYNA keyword \*CONSTRAINED\_LAGRANGE\_IN\_SOLID. Three such coupling interfaces are defined one for the lower air, sand and explosive products; the upper air is not coupled to the Lagrange target plates. The keyword parameters were default values with the exception of DIREC=2 normal direction, compression only and ILEAK=1 weak — leakage control is turned off if the penetrating volume fraction > FRCMIN+0.1.

The material models and parameters are provided in an Appendix.

## 4.2 Results Comparisons

Table 7 is an update of the previously presented Table 6. The results from the SwRI CTH and present LS-DYNA MM-ALE 3D simulations are also included along with the previously presented experimental and \*INITIAL\_IMPULSE\_MINE results. The present 3D MM-ALE results provide an indication of the accuracy that can be achieved using a so called first principals methods compared with those reported previously for the engineering model, i.e. \*INITIAL\_IMPULSE\_MINE.

The present 3D MM-ALE results provide surprisingly good correlation with the SwRI experiments. The largest relative error occurs for the 180-degree (horizontal) target plate where the impulse is over predicted by about 12%. Interestingly, the axisymmetric (AS) version of this model provided an impulse that only over predicted the SwRI experimental result by 5%. For the 120 and 90-degree targets plates, the 3D MM-ALE predicted impulses are 2% and less than 1% greater, respectively than the SwRI experiments. Such close agreement with the experiments needs further study via mesh refinement studies and domain size changes, as reported in the appendix describing the axisymmetric modeling.

The SwRI 3D simulation results, for other than the 180-degree plate, do not reflect the same degree of agreement with the experiments as the present results. Some reasons for the disagreement with the experimental results are presented in Anderson et al. (2010).

Figure 7 shows the vertical velocity histories of the three target plates computed using the present 3D MM-ALE models described above. As discussed previously, the 180-degree plate provides more confinement of the soil ejecta and detonation products than the two included angle plates, and hence has a larger vertical velocity. Similarly, the 120-degree plate provides slightly more confinement than the 90-degree plate and hence has a larger vertical velocity than the 90-degree plate.

Table 7 Comparisons of SwRI, IIM and 3D MM-ALE vertical velocity and impulses.

180	Velocity (m/s)	RE	Impulse (kg-m/s)
SwRI	6.60		1979.33
3D	6.98	0.06	2094.00
IIM			
Shells	10.09	0.53	3027.48
Solids	10.09	0.53	3027.50
MM-ALE			
3D	7.40	0.12	2231.80
AS	6.90	0.05	2078.60
120	Velocity (m/s)	RE	Impulse (kg-m/s)
SwRI	3.81		1181.67
3D	5.45	0.43	1686.23
IIM			
Shells	4.34	0.14	1342.76
Solids	4.34	0.14	1342.76
MM-ALE			
3D	3.90	0.02	1207.32
90	Velocity (m/s)	RE	Impulse (kg-m/s)
SwRI	2.63		812.33
3D	4.22	0.60	1305.67
IIM			
Shells	2.07	-0.21	639.32
Solids	2.07	-0.21	639.12
MM-ALE			
3D	2.64	0.00	814.08

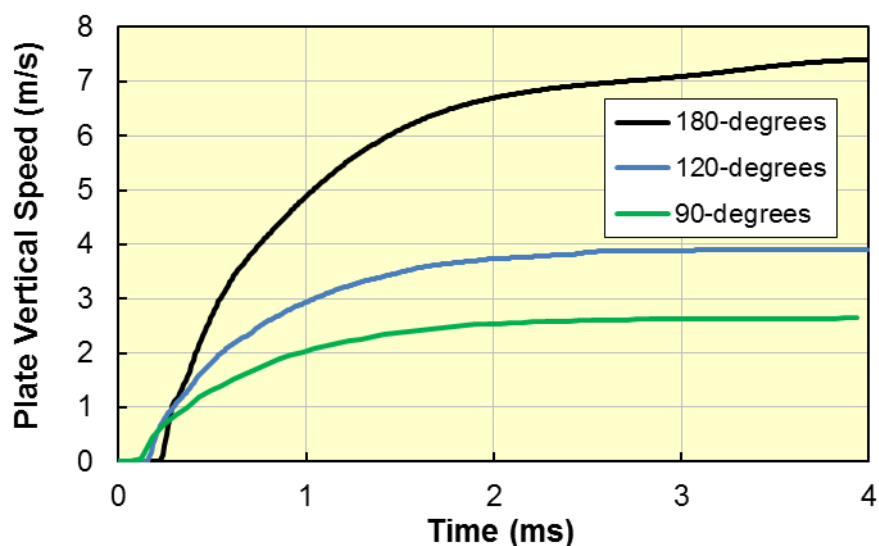


Figure 7 Vertical velocity histories of three target plate configurations from the 3D models.

Figure 8 shows models of the three SwRI buried charge and plate configurations: initial, 1.53 and 4ms. The images provide a graphic illustration of the deflection of the detonation products (red). The air (blue) and small amount of soil (green) above the charge 'disappears' as the jet of detonation products

reaches the target plates, i.e. the detonation products become the dominant fluid interacting with the target plates in the MM-ALE simulation.

These deformed geometry figures also indicate that including the reinforcing ring near the top of the Sonotube might provide a 'choke point' or 'throat' for the detonation products to pass through and further restrict the lateral expansion of the soil. Including a model of the Sonotube would be interesting; however developing such a frangible material model might be more effort than it is worth.

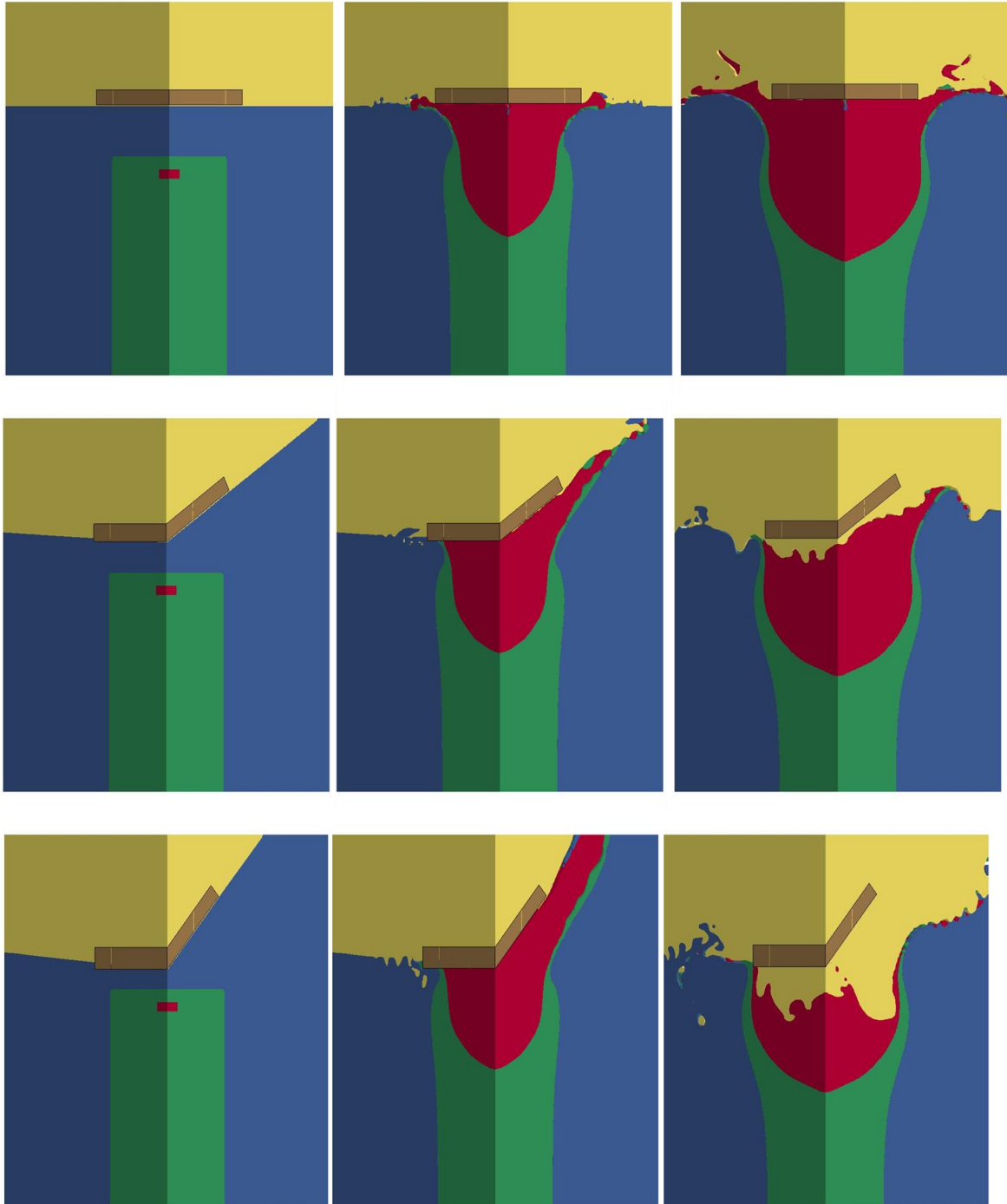


Figure 8 Initial (left column), 1.53ms (center column) and 4ms (right column) configurations of the three plates: 180-degree (top), 120-degree (middle), and 90-degree (bottom).

## 5 Summary

An engineering model applicable to buried charges based on the experiments of Westine et al. (1985) and analytical extension to angled plates by Tremblay (1998) has been presented. The LS-DYNA implementation of the model was verified via comparisons with the analytical solutions of Tremblay to several problems of interest.

The excellent buried charge experiments by SwRI, Anderson et al. (2011), were used as validation experiments in comparisons with both the \*INITIAL\_IMPULSE\_MINE engineering model and detailed coupled 3D MM-ALE simulations. The engineering model performed surprisingly well for the angled target plates and was within the stated accuracy limits provided by Westine et al. The 3D MM-ALE simulation results also compared well to the experimental results with a maximum relative error of 12% for the 180-degree target plate.

It is believed that this engineering model of buried charge impulse will be very effective in reducing CPU time during the initial stages of structures subject to land mine and IED explosions. For example, the 3D MM-ALE model required a simulated duration of about 3.5ms to attain the maximum momentum of the plate with a corresponding CPU time of about 22 hours. The corresponding \*INITIAL\_IMPULSE\_MINE model only required 2 minutes on the same computing platform.

## 6 References

Anderson, C.E. Jr., T. Behner, and C.E. Weiss (2011), "Mine Blast Loading Experiments," *International Journal of Impact Engineering*, Volume 38, page 697-706.

Anderson, C.E. Jr, R.P. Bigger, T. Behner, C.E. Weiss, and S. Chocron, (2010), "Mine-Blast Loading: Experiments and Simulations," ARL Research in Ballistic Protection Technologies Workshop, Booz Allen Hamilton Conference Center, Herndon, VA May 24 – 26.

McGlaun, J.M., S.L. Thompson, and M.G. Elrick, (1990) "CTH: A Three-Dimensional Shock Wave Physics Code," *International Journal of Impact Engineering*, Volume 10, pages 351-360.

Roache, P. (2009), "Fundamentals of Verification and Validation," Hermosa Publishers, Albuquerque, NM.

Westine, P.S., B.L. Morris, P.A. Cox, and E.Z. Polch, (1985) "Development of Computer Program for Floor Plate Response from Land Mine Explosions," Technical Report No. 13045, US Army Tank-Automotive Command, Warren, MI, UNCLASSIFIED LIMITED DISTRIBUTION.

Tremblay, J. E., (1998) "Impulse on Blast Deflectors from a Landmine Explosion," Defence Research Establishment Valcartier (Quebec), Technical Report DREV-TM-9814, Accession Number: ADA482742

Williams, K, and S. McClennan (2002) "A Numerical Analysis of Mine Blast Effects on Simplified Target Geometries: Validation of Loading Models," Defence Research Establishment Valcartier (Quebec), Technical Report 2002-206.

[<http://pubs.drdc.gc.ca/PDFS/unc69/p519140.pdf>]

[[http://www.dynalook.com/international-conf-2002/Session\\_6-5.pdf](http://www.dynalook.com/international-conf-2002/Session_6-5.pdf)]

Smith, P.D. and J.G. Hetherington, "Blast and Ballistic Loading of Structures," Butterworth-Hineman, (ISBN: 0750620242), 1994.

Dobratz, B.M. and P.C. Crawford (1985) "LLNL Explosives Handbook Properties of Chemical Explosives and Explosive Simulants," Lawrence Livermore National Laboratory, UCRL-52997 Change 2.

Wenzel, A.B and E.D. Esparza, "Measurements of the Pressure and Impulses at Close Distances from Explosive Charges Buried and in Air," SwRI Contract No. DAAK02-71-C-0398 with MERDC, 21 August 1972.

## 7 Appendix – Keyword \*INITIAL\_IMPULSE\_MINE

The keyword \*INITIAL\_IMPULSE\_MINE description provided in this section is intended to provide the present manuscript reader with an easily accessible description. Refer to the latest LS-DYNA User Manual for the most recent description of this keyword and its parameters.

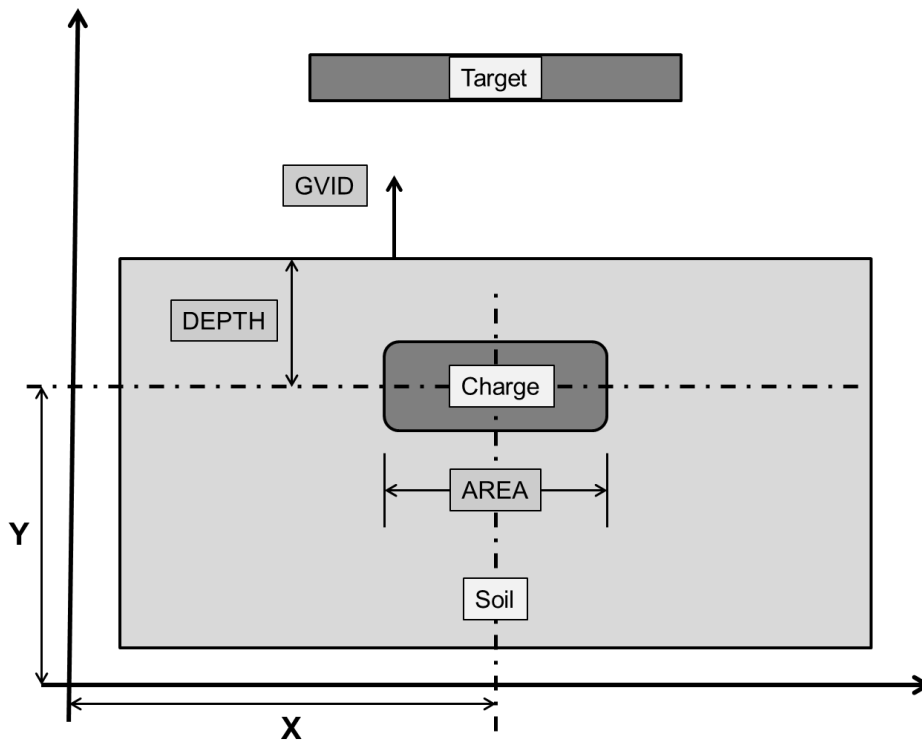


Figure 9 Schematic of \*INITIAL\_IMPULSE\_MINE keyword parameters.

Figure 9 is a schematic of the primary geometric parameters associated with the keyword \*INITIAL\_IMPULSE\_MINE. An example of the keyword input was given previously and is repeated here:

```
*INITIAL_IMPULSE_MINE
$  SSID      M      RHOS     DEPTH     AREA     SCAL (not used)  UNIT
   333,  6500.0,  1.60E-3,  70.0,  55.15E3,  0.0,           ,    6
$   X       Y       Z      NIDMC    GVID     TBIRTH     PSID     SEARCH
   0.0, -70.0,  0.0,    0,     222
```

**SSID** Segment set ID  
**M** Equivalent mass of TNT  
**RHOS** Density of overburden soil.  
**DEPTH** Burial depth from the ground surface to the center of mine.  
**AREA** Cross-sectional area of the mine.  
**SCAL** Impulse scale factor.  
**UNIT** Unit system.  
 EQ.1: inch, dozen slugs (i.e., lbf-s<sup>2</sup>/in), second, psi (default)  
 EQ.2: meter, kilogram, second, Pascal  
 EQ.3: centimeter, gram, microsecond, Megabar  
 EQ.4: millimeter, kilogram, millisecond, GPa

---

	EQ.5: millimeter, metric ton, second, MPa
	EQ.6: millimeter, gram, millisecond, MPa
<b>X</b>	x-coordinate of the mine center.
<b>Y</b>	y-coordinate of the mine center.
<b>Z</b>	z-coordinate of the mine center.
<b>NIDMC</b>	Optional node ID representing the mine center (see *NODE). If defined then X, Y, and Z are ignored.
<b>GVID</b>	Vector ID representing the vertically upward direction, i.e., normal to the ground surface (see *DEFINE_VECTOR).
<b>TBIRTH</b>	Birth time. Impulse is activated at this time.
<b>PSID</b>	Part set ID identifying parts affected by the mine. If zero it defaults to the part comprised of the nodes of the segment set.
<b>SEARCH</b>	Limit search depth into the plate. Initial nodal velocity is distributed from the segment to a depth equal to the <b>SEARCH</b> value.

## 8 Appendix — LS-DYNA Axisymmetric Modeling

This section focuses on the axisymmetric modeling of the SwRI experiments, including the overall size of the computational domain and mesh refinement.

### 8.1 Computational Domain

The geometry of the physical components: sand, COMP-B explosive charge and target plates, are specified by the experiments. The primary numerical geometry parameter is the extent of the Eulerian mesh, i.e. the radius and height of the axisymmetric model. Each of the three axisymmetric target plate configurations was simulated using several Eulerian computational domains, in addition to mesh refinements.

Each of the three target plate configurations required a slightly different (optimal) computational domain. Since the size of the computational domain affects the total CPU time, an optimal domain is one that is not too small as to affect the computed results and not too large as to be excessively CPU costly. The flat plate configuration deflects the energy horizontally and requires a sufficiently large radius. The 90 degree target configuration deflects energy vertically and radially, but not equally despite the 45 degree angle to the flow. The 120 degree target plate, while similar to the 90 degree configuration, deflects more energy radially than vertically.

For the purposes of illustration, the computational domains considered for the 120 degree target plate are presented. Using a uniform fixed mesh size of 8mm, four computational domains, i.e. background meshes, were investigated; the target plate mesh was also discretized at 8mm to provide nearly<sup>3</sup> equal mesh sizes between the fluid and structure domains. Figure 10 shows the four computational domains at the same scale, i.e. they can be directly compared. The domain size is listed above each configuration, radius and height, along with the number of elements in the background mesh. Note: the air mesh is divided into two parts (yellow & blue) to better observe Fluid-Structure Interaction (FSI) leakage.

---

<sup>3</sup> The 120 degree target plate mesh is on a 60 degree angle to the fluid mesh, so the meshes do not align.

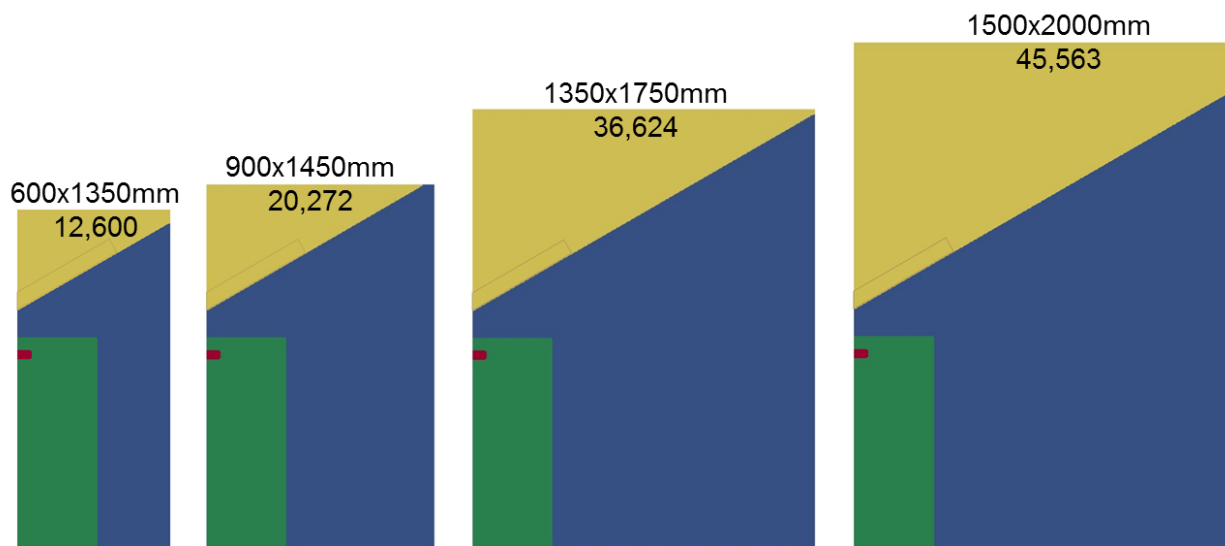


Figure 10 Illustration of four computational domains investigated for the 120 degree target plate using 8mm mesh spacing.

Table 8 presents the computed 120-degree target plate momentum for the four background domains with uniform 8mm mesh. As can be seen in this table, as the size of the domain increases the target plate moment decreases. The relative difference in target plate momentum between successive domains is about 1%, and about 2% from the smallest to largest domains.

Table 8 Summary of 120-degree target plate momentum for four computational domains using 8mm mesh spacing

Domain (mm)	Momentum (kg-m/s)
600x1350	797.87
900x1450	793.29
1350x1750	789.56
1500x2000	781.23

Since these 120-degree target plate configuration momentum results are for an axisymmetric simulation, they cannot be directly compared to the average experimental measurement of 1183 kg-m/s. Unfortunately, SwRI did not report their axisymmetric model results for the 120 degree target plate configuration, so no code-to-code comparison can be made.

## 8.2 Mesh Refinement

Having estimated an optimal computational domain, a mesh refinement study was conducted to establish a rate of grid convergence based on the target plate momentum.

### 8.2.1 Horizontal Target Plate

For the horizontal plate case, for which the axisymmetric model results can be directly compared with the experimental measurement of 1979 kg-m/s (or 1979 N-s, or 1979 kN-ms) three mesh refinements were considered: 8, 4 and 2mm uniform background and target plate meshes. The computed horizontal plate momenta are listed in Table 9.

Table 9 Summary of flat plate mesh refinement study

Mesh Size (mm)	Domain (mm)	Momentum (kg-m/s)
8	600x1250	2078.6
8	1200x1250	2088.6
<b>8</b>	<b>1400x1500</b>	<b>2142.5</b>
4	600x1250	1917.7
4	1200x1250	1933.6
<b>4</b>	<b>1400x1500</b>	<b>1930.9</b>
2	600x1250	1871.4
<b>2</b>	<b>1400x1500</b>	<b>1885.9</b>

For the largest computational domain considered, i.e. 1400x1500mm, results for all three mesh refinements were computed, see Table 9. These three mesh refinement results can be used with the Grid Convergence Index, Roache (2009), to estimate both the rate of convergence of 1.55 and an estimate of the numerically exact solution 1861 kg-m/s; the numerically exact solution is the solution to which the model appears to be converging. Figure 11 shows the results of the mesh convergence study for the horizontal plate along with the experimental measurement — displayed with one standard deviation vertical error bars.

The estimated numerically exact plate impulse of 1861 kg-m/s under predicts the measured plate impulse of 1979 kg-m/s by 6%, which may be viewed as an acceptable error considering no calibrating of the COMP-B, nor sand, model was performed.

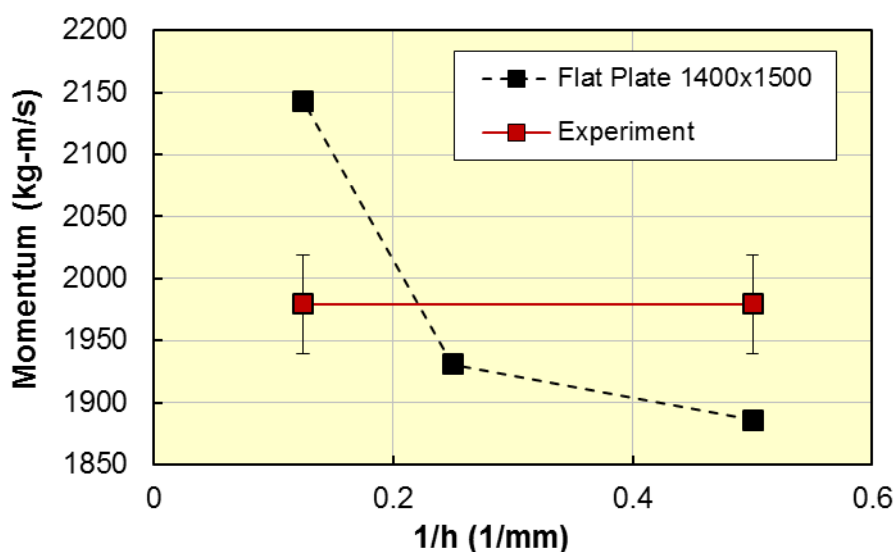


Figure 11 Horizontal plate mesh convergence study results and comparison with the experimental measurement.

### 8.2.2 120-degree Target Plate

For the 120-degree included angle target plate, again three mesh refinements were considered: 8, 4 and 2mm of the uniform background and target plate meshes, see Table 10. All three uniform mesh sizes were used with the 1350x1750mm computational domain. Figure 12 shows the results of the mesh convergence study for the 120-degree target plate. For this mesh triplet, the rate of convergence was 1.31 and the estimated numerically exact target plate impulse was 766 kg-m/s.

Table 10 Summary of 120 degree target plate mesh refinement study

Mesh Size (mm)	Domain (mm)	Momentum (kg-m/s)
8	600x1350	797.87
8	900x1450	793.29
<b>8</b>	<b>1350x1750</b>	<b>789.56</b>
8	1500x2000	781.23
4	600x1250	747.13
<b>4</b>	<b>1350x1750</b>	<b>746.73</b>
2	600x1250	772.82
<b>2</b>	<b>1350x1750</b>	<b>758.25</b>

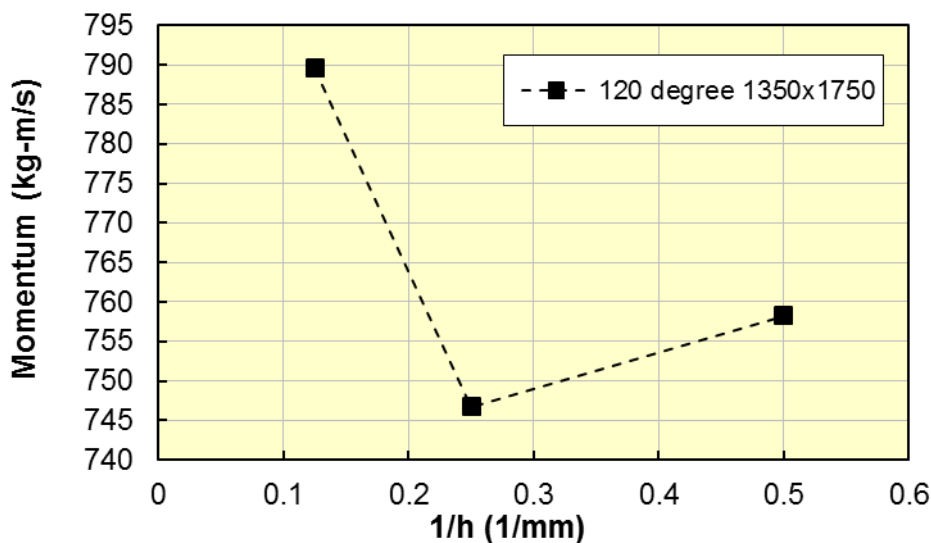


Figure 12 Included angle of 120 degrees target plate mesh convergence study results.

### 8.2.3 90-degree Target Plate

For the 90-degree included angle target plate, once again three mesh refinements were considered: 8, 4 and 2mm for the uniform background and target plate meshes, see Table 11. All three uniform mesh sizes were used with the 1350x1750mm computational domain. Figure 13 shows the results of the mesh convergence study for the 90-degree target plate. For this mesh triplet, the rate of convergence was only 0.55 and the estimated numerically exact target plate impulse was 355 kg-m/s. For this low convergence rate of 0.55 it is likely the results are not representative of asymptotic convergence which is required for using the Grid Convergence Index.

Table 11 Summary of 90-degree target plate mesh refinement study

Mesh Size (mm)	Domain (mm)	Momentum (kg-m/s)
8	600x1350	477.91
<b>8</b>	<b>1350x1750</b>	<b>464.59</b>
8	1500x2000	458.42
4	600x1250	423.92
<b>4</b>	<b>1350x1750</b>	<b>425.40</b>
4	1550x2500	426.05
2	600x1350	839.07
<b>2</b>	<b>1350x1750</b>	<b>402.89</b>
2	1500x2500	400.53

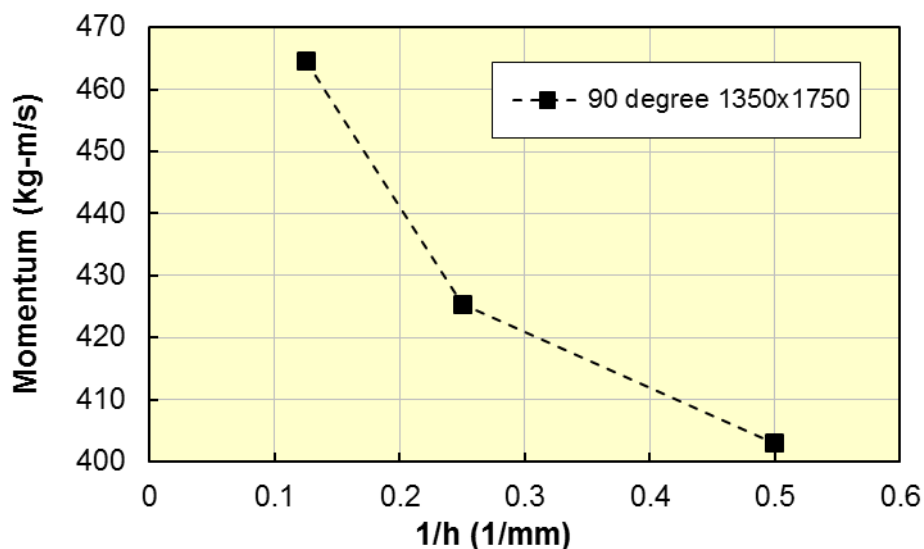


Figure 13 Included angle of 90-degrees target plate three mesh convergence study results.

A fourth mesh refinement of 1mm was subsequently performed using the 1350x1750mm domain. The computed impulse was 391.70 kg-m/s. Using the 4, 2, and 1mm mesh triplet the convergence rate is still low at 0.70 and the estimated numerically exact impulse is 373 kg-m/s. Figure 14 shows the four mesh momentum convergence.

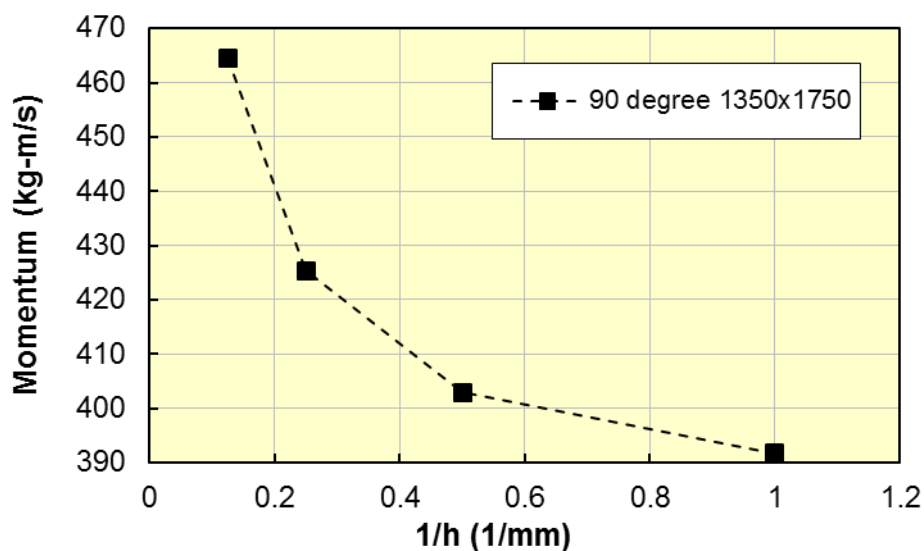


Figure 14 Included angle of 90-degrees target plate four mesh convergence study results.

Interestingly, SwRI also reported a slow convergence rate for the 90-degree target plate in their axisymmetric simulations. Their report provides a plot of plate momentum histories for mesh sizes ranging from 250mm to 1.25mm with the finest mesh plate momentum of about 680 kg-m/s. The SwRI numerical result is significantly larger than the present estimated 373 kg-m/s. The SwRI axisymmetric result seems oddly large when compared to the measured impulse of 812 kg-m/s considering the difference in maximum projected areas of the axisymmetric cone at  $0.32\text{m}^2$  and the 3D target plate at  $0.51\text{m}^2$  an area ratio of 1.6

An oddity of the 90-degree target plate mesh refinement study was the impulse result for the 2mm mesh, with the smallest computational domain of 600x1350mm. For this configuration, the computed plate impulse is 839 kg-m/s, which is essentially double all the other computed impulses for the 90 degree plate. The reason for this numerical 'outlier' is undetermined.

## 9 Appendix - Material Models and Parameters

The basic system of units for these input parameters is grams-millimeter-milliseconds with a derived stress unit of MegaPascal.

### 9.1 Air

```

$
*MAT_NULL
$ MID RO PC MU TEROD CEROD YM PR
  100, 1.29e-6, 0.0, 0.0, 0.0, 0.0, 0.0

*EOS_Linear_Polynomial
$ EOSID C0 C1 C2 C3 C4 C5 C6
$ 100 , -0.1, 0.0, 0.0, 0.0, 0.4, 0.4, 0.0
  100 , 0.0, 0.0, 0.0, 0.0, 0.4, 0.4, 0.0
$ e0 v0
  0.25, 1.0

```

### 9.2 COMP-B

```

*MAT_HIGH_EXPLOSIVE_BURN
$ MID RO D PCJ BETA
  1080, 1.717E-3, 7.98e3, 2.95E4, 0.0

*EOS_JWL
$ EOSID A B R1 R2 OMEG E0 V0
  1080 , 5.242E5, 7.678E3, 4.2, 1.10, 0.34, 8.5E3, 1.0

```

### 9.3 Sand

```

*MAT_ELASTIC_PLASTIC_HYDRO_SPALL
$ MID RHO G SIGY EH PC FS CHARL
  30010, 1.37E-03, 76.9, 0.0, 0.0, -6.9e-3, 0.0, 0.0
$ A1 A2 SPALL
  1.39642, 0.0, 3.0
$-----1-----2-----3-----4-----5-----6-----+-----
-7-----+-----8
$ EPS1, EPS2, EPS3, EPS4, EPS5, EPS6, EPS7, EPS8

$ EPS9, EPS10, EPS11, EPS12, EPS13, EPS14, EPS15, EPS16

$ ES1, ES2, ES3, ES4, ES5, ES6, ES7, ES8,

$ ES9, ES10, ES11, ES12, ES13, ES14, ES15, ES16

*EOS_TABULATED_COMPACTION
$ EOSID GAMA E0 V0 LCC LCT
  30010, 0.0, 0.0, 1.0
$ EV1 EV2 EV3 EV4 EV5

```

---

	0.000,	-0.113,	-0.176,	-0.247,	-0.296
\$ EV6	EV7	EV8	EV9	EV10	
	-0.352,	-0.395,	-0.433,	-0.467,	-0.470
\$ P1	P2	P3	P4	P5	
	0.00,	14.98,	29.15,	58.18,	98.10,
\$ P6	P7	P8	P9	P10	
	179.44,	289.44,	450.20,	650.66,	800.0
\$ T1	T2	T3	T4	T5	
	0.0,	0.0,	0.0,	0.0,	0.0
\$ T6	T7	T8	T9	T10	
	0.0,	0.0,	0.0,	0.0,	0.0
\$					
\$ K1	K2	K3	K4	K5	
	157.9e3,	157.9e3,	157.9e3,	157.9e3,	157.9e3
\$ K6	K7	K8	K9	K10	
	157.9e3,	157.9e3,	157.9e3,	157.9e3,	157.9e3